

Device Simulation of Monolithic Active Pixel Sensors: Radiation Damage Effects

Nicolas T. Fourches, *Senior Member, IEEE*

Abstract—Vertexing for the future International Linear Collider represents a challenging goal because of the high spatial resolution required. CMOS Monolithic Active Pixel Sensors (MAPS) represent a good potential solution for this purpose. Up to now many MAPS sensors have been developed. They are based on various architectures and manufactured in different processes. However, up to now, the diode sensor has not been the subject of deep investigation. This is a cause for concern because the physical basis of such sensor is the partially depleted diode hit by minimum ionizing particles, in which the physical mechanisms for signal formation are not rigorously established. This is partly due to the presence of an important diffusion component in the charge transport. We present here simulations mainly based on the S-PISCES code, in which physical mechanisms affecting transport are taken into account. Diffusion, influence of residual carrier concentration due to the background doping level, and more importantly charge trapping due to deep levels in the active (detecting) layer are studied together with geometric aspects. The effect of neutron irradiation is studied to assess the effects of deep traps. A comparison with available experimental data, obtained on processed MAPS before or after neutron irradiation will be introduced. Simulated reconstruction of the Minimum Ionizing Particle (MIP) point of impact in two dimensions was also investigated. For further steps, guidelines for process choices of next Monolithic Active Pixel Sensors are introduced.

Index Terms—MAPS, radiation damage, defect, device simulation, neutrons, PISCES, CMOS

I. INTRODUCTION

SIMULATION of Monolithic Active Pixel Sensors (MAPS) was the first step forward for the development of the MIMOSAn series of prototypes [1][2] and other similar chips. The feasibility of such detecting arrays was then demonstrated using device simulation and subsequently confirmed by measurements on manufactured chips. As a charged particle detector with a micrometer range, spatial resolution is a major issue for the μ vertex detectors of future linear colliders or other accelerator experiments. Optimization of the MAPS operation in their future environment raises a number of questions. First the impact of material quality more or less affected by irradiation (both ionizing and neutral) on the performance of MAPS must be addressed on the basis of material models feeding simulation codes in order to make

valid comparisons with measured results on manufactured chips. Second, these data and their conclusions should be the basis for simulation studies of basic problems posed by MAPS designed for charged particle detection. Among them, active layer thickness optimization, pixel pitch determination, doping level thresholds in the detecting layer together with defect density thresholds, are the most critical issues.

II. DAMAGE IN THE SENSITIVE MATERIAL

Some measurements have been recently performed on MIMOSAn chips irradiated with ionizing radiation or fast neutrons [3]. The radiation generates point defects or displacement damage in the silicon material, which acts as the sensitive medium. (i.e. a detecting medium). Deep traps greatly affect charge collection. More importantly primary displacements produced by fast neutrons are an excellent tool to transform a defect free material into a material containing a concentration of point and extended defects to the extent (at high fluences) of total amorphization, in the present case of c:Si. Such is not the case here since most of the applications we are looking to will take place in a fluence range such that the defect concentration will not exceed 10^{13} defects/cm³. A most notable exception is the CBM experiment at GSI for which the displacement damage level could exceed 10^{15} deep defects/cm³ [4]. If MAPS are to be one of the universal answers to vertexing in future experiments (hadron and lepton colliders or fixed target experiments) displacement damage in MAPS has to be fully understood. Moreover the side effect of such studies is a better understanding of charge transport in the native material constituent of MAPS, and the effects of defects on charge collection, this leading to good initial process and material choices, and adequate layout techniques. A plot of the experimental charge collection efficiency calculated on nine pixels clusters has been published and presented versus neutron fluence (see [3] Fig. 7).

A. Simulation Model

Electrically active defects tend in c:Si to have an introduction rate for neutrons at 300 K of a few cm⁻¹. Most recent studies on high resistivity silicon material have been based on TSC (Thermally Stimulated Currents), DLTS (Deep Level Transient Spectroscopy) and TCT (Thermally induced Transient Currents) to characterize deep traps [5-20]. Typical DLTS spectra of neutron-irradiated silicon have been published recently demonstrating the general picture of silicon irradiated with fast neutrons. Intrinsic defects seem to be

Manuscript received February, 2009. This work was supported by the Commissariat à l'Énergie Atomique (France).

Nicolas T. Fourches is with the Commissariat à l'Énergie Atomique, CEN Saclay, DSM/IRFU/SEDI/LDEF (telephone: 0033169086164, e-mail: nicolas.fourches@cea.fr).

dominant. Detailed understanding of displacement induced deep defects requires the knowledge of the carrier capture kinetic. Past measurements made on germanium show that the capture kinetic is altered by the presence of extended defects [21], a similar conclusion being seemingly valid for silicon [9]. Local variation of the free carrier concentration near the damaged region (whether described by the Gossick model or an alternative simple model [21]) is the main origin of the carrier capture kinetic variations. In silicon defects observed after neutron irradiation at room temperature are mostly vacancy-complexes, divacancies, either isolated or in clusters. In p-silicon carrier capture of majority carrier seem should be enhanced in neutron irradiated material due to the increase of shallow acceptors concentration just like in p-type neutron irradiated germanium. Cluster-type defects have a negative charge core in n-type silicon that would attract in principle positive holes. Hence, in p-type silicon, near the core but outside it, the hole concentration would be enhanced inducing an increased capture rate for hole traps. The charged state of the isolated electron traps is then positive or neutral leading to fairly high capture cross sections for minority carriers (electrons) at least when these defects behave “regular” properties (no bistability, no negative correlation energy). In-core deep defects have a limited influence, as there charge state cannot be much changed due to the above-mentioned coulombic effects. However, they result in an under-evaluation of the deep-defect concentration, by DLTS measurements for instance [9]. Another satisfactory model, which was originally proposed for germanium [21], is that the neutron irradiation induces defects that give rise to shallow acceptors and deep levels inside an extended defect dense region, this enhances the hole concentration near the region and the same conclusions hold for the capture kinetics. In addition this model is consistent with the type inversion observed earlier in n-type neutron irradiated silicon (and in germanium). The hole density increases after neutron irradiation in p-type material, proving the need of extra shallow acceptor states. This model does not preclude the existence of clusters of defects in the defect dense region; polyvacancies can be distributed into it without making the assumption of a strong core electrostatic effect. To remain conservative, the neutron irradiated silicon material can be reduced in a transport simulation model to a deep level rich material with a given introduction rate and enhanced capture cross sections. Deep levels from [6-11,16] and their capture cross sections are given in table I with their respective introduction rates. In the S PISCES (2D) code, drift/diffusion transport with trapping and emission of carriers are taken into the model.

TABLE I
CHARACTERISTICS OF THE TRAPS CONSIDERED IN THE MODEL
FROM THE LITERATURE (FLE [8, 9], FRE [10, 11], ERE [6, 7], MOL [16])

Traps considered	Capture cross sections	Introduction rate	Reference
$E_c - 0.46$ eV	Equivalent electron cross section $\sigma_e = 10^{-13}$ cm ²	1 cm ⁻¹	FLE, MOL
$E_c - 0.18$ eV	Equivalent electron cross section $\sigma_e = 10^{-13}$ cm ²	1 cm ⁻¹	FRE
$E_c - 0.25$ eV	Equivalent electron cross section $\sigma_e = 10^{-13}$ cm ²	0.5 cm ⁻¹	FLE, MOL
$E_v + 0.36$ eV	Equivalent hole cross section $\sigma_h = 10^{-13}$ cm ²	1 cm ⁻¹	ERE

Two-dimensional simulation is sufficient to describe the behaviour of the MAPS since a sheet of one μm is in fact taken into consideration. In fact, simple considerations show that the detrimental effects due to carrier migration and trapping should be enhanced with three-dimensional simulation, inducing worsened and more pronounced results for a large structure in a two-dimensional simulation. The effects then appearing in 2D simulations would then be quite predictive of what should be taking place in the real world.

B. Simulation structures and preliminary conclusions

The simulation structures used in this study are simple n+pp+ structures comprising three abutted pixels. These form a 3-pixel cluster, which is the reduction in 2D of the 9-pixel clusters currently used in the real world and in 3D simulations. The readout is an electrode biased by a resistor (Fig. 1).

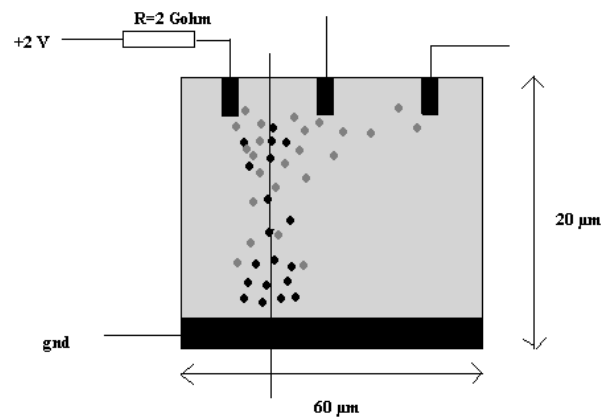


Fig 1: Sketch of one of the three pixels structure used for the simulations. Bias at the top of the 5 Gohm resistor: 2 V for all the n+ electrodes (only one shown). Electron-hole pairs generated along vertical particle track are represented. Electrons (grey) migrate towards the n+ well. A relatively high active layer thickness (ALT) is taken.

We have chosen to let the p region be the active region, or the epi-layer in the real world. The thickness of the active layer, the pitch of the pixel, the doping density and of course the trap concentration are then parameters used for the simulation. The first study was made to evaluate the effect of the doping level in the active layer. Fig. 2 and 3 show that the total charge collected on the three electrodes is reduced when the p doping density increases this when all other characteristics and biases are kept equal. This first study leads to an upper limit on the doping density in the active layer that should not exceed 10^{16} cm⁻³ for adequate operation of present day MAPS pixels. Higher doping densities result, in a limited depleted zone around the upper n-well electrode, and hence a reduced drift component in the total signal. Higher doping densities mean a reduced diffusion contribution for the minority carriers ($\Delta n/p$ decreases). For MAPS with a limited concentration of deep defects in the active layer, the total signal is proportional to the

generation rate along the track in the range studied (two orders of magnitude above the MIP ionization (generation) rate).

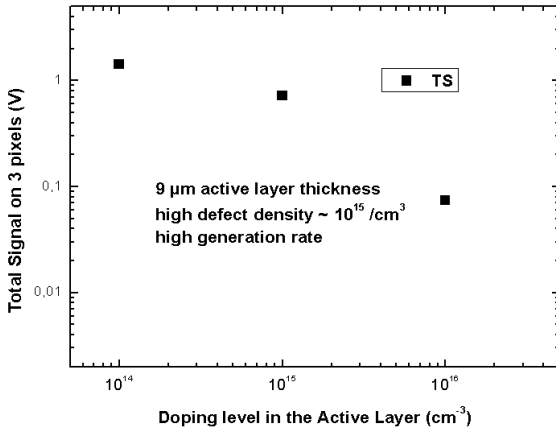


Fig 2: Total signal on three pixels (TS) plotted versus doping level in the active layer for a thickness of 9 μm and a defect density of $\sim 10^{15}\text{cm}^{-3}$. The generation rate corresponds to approximately 10 MIPs across the structure. The scales are log scales. Bias at the top of the 5 Gohm resistor: 2 V

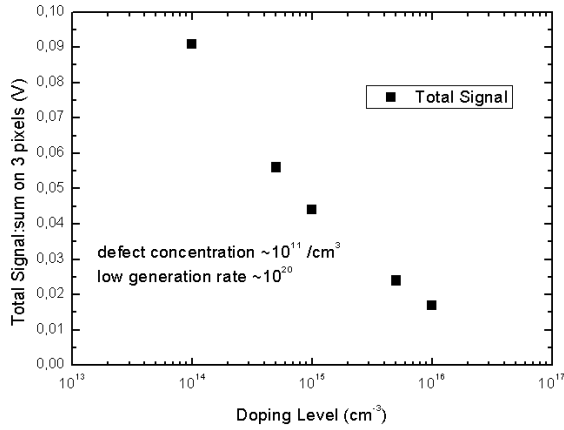


Fig 3: Total signal versus active layer thickness for a low defect concentration $\sim 10^{11}\text{cm}^{-3}$. The active layer thickness is 11 μm and the generation rate is close to that of a MIP (80 e-/ μm). Same bias as in Fig. 1.

III. RESULTS

A. Role of the active layer thickness

The active layer thickness is an important parameter for charge generation and collection. The naïve approach is to estimate the total signal as a growing function of the thickness of the active layer, because the generated charge is proportional to the active layer thickness (along a MIP track). Assuming this, one is tempted to increase the active layer thickness in order to obtain an increased signal. Simulations do not confirm this approach. With reasonable assumptions this approach only holds when the deep defect concentration is extremely low (i.e.: no charge is trapped during transport), with the restriction that although linear the total charge only grows slowly with the active layer thickness. No proportionality is ever observed (Fig.4).

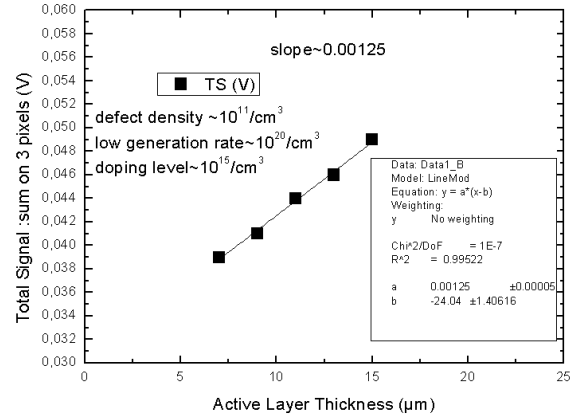
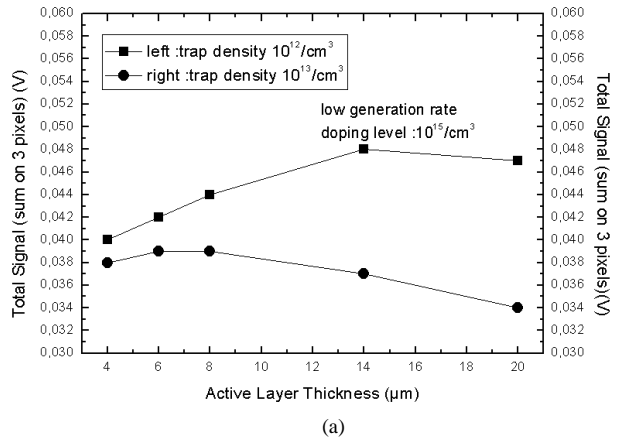


Fig.4: Total signal is plotted versus Active layer Thickness for a low defect density $\sim 10^{11}\text{cm}^{-3}$. The generation rate corresponds to a MIP and the doping level is $\sim 10^{15}\text{cm}^{-3}$. The slope is sub-proportional to the active layer thickness.

When the defect concentration increases, the total charge is not a monotonous function of the active layer thickness. In some cases the signal reaches a plateau and decreases as the active layer thickness rises (Fig. 5(a)). This is due to the effects of high defect densities for a given pixel geometry. Low pixel active layer thicknesses have the advantage of a confinement effect that results in an enhanced signal. Increasing the active layer thickness reduces this confinement effect. This explains qualitatively the decrease of the observed total signal when the active layer thickness rises above a threshold.



(a)

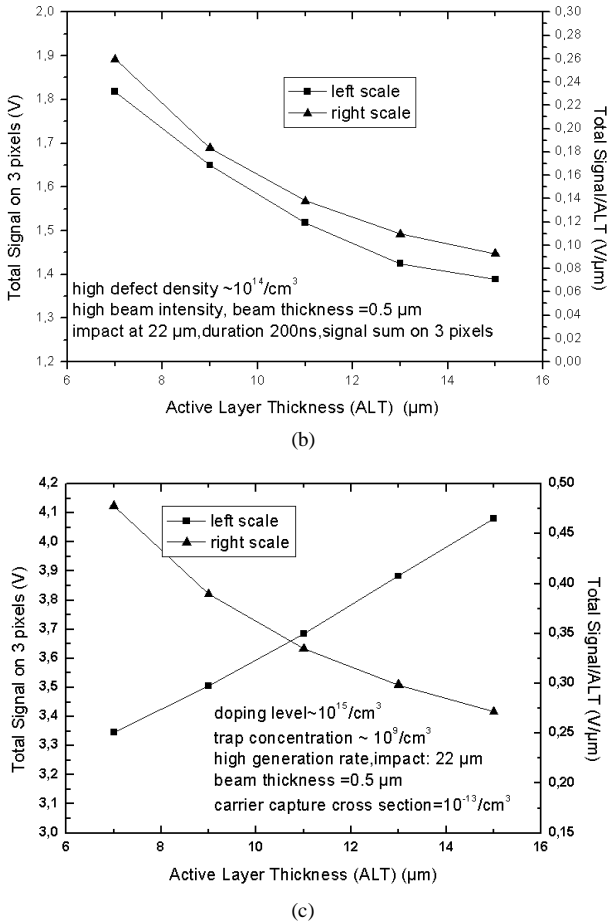


Fig. 5: Total Signal versus active layer thickness for three neutron induced different defect densities (a) At moderately high defect densities $\sim 10^{13}/\text{cm}^{-3}$ the Total signal levels off and decays for thicknesses above 8 μm. (b) At high defect densities $\sim 10^{14}/\text{cm}^{-3}$ the total signal decays as the thickness is increased. (c) At very low defect densities $\sim 10^9/\text{cm}^2$, the total signal increases monotonously with active layer thickness. ALT is the active (epi) layer thickness.

The effect is very pronounced at high deep defect density where a monotonous decrease of the total signal with active layer thickness is observed (Fig 5(b)). This is because the deep defect density exceeds the doping density, the deep defects controlling the carrier concentration. Hence simulated type inversion can occur in the un-depleted zone and this may contribute negatively to the total signal.

B. Measured Results

Many measured results have been obtained on MAPS. Recent published data [22-23] confirm the effects predicted by simulation of the active layer thickness influence on total signal build up. Manufactured chips of different technologies and different pixel configurations show that there is an overall CCE decrease versus active layer thickness (Fig. 6). These data were obtained with in-lab ^{55}Fe tests. This is consistent with our simulations made with a deep defect concentration ranging within $10^{12}-10^{13} \text{ cm}^{-3}$. This concentration range is consistent with what is expected in the native epitaxial layers

grown on silicon, although the deep levels may be of a different nature compared with the neutron induced deep defects (they still have mainly a vacancy origin). The same conclusion holds for the effect of active layer thickness. In this case, the total charge generated does not increase above a threshold, which lays around 14 μm in this case. This could indicate that, being consistent with the simulated results, the quality of the active layer (epi-layer here) is not as good as it may be expected, due to a high native defect concentration due to the epitaxial processing.

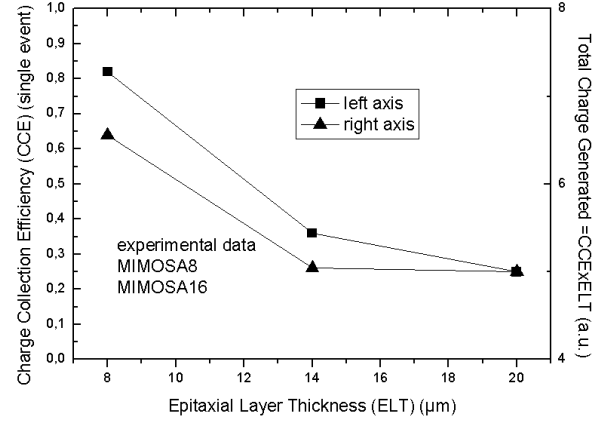


Fig. 6: Measured Charge Collection efficiency plotted versus Epi-Layer thickness (ELT). The data were taken out of ref 22 and 23. The right scale shows an estimation of the total charge generated which is proportional for a MIP to the CCE x Epi Layer Thickness. The total signal does not increase with epi-layer thickness. These are un-irradiated sample chips.

C. Simulated Influence of the Impact Location

The impact location of the track has a great influence on the charge split between the three collecting electrodes. The track of the particle is assumed to be vertical. Fig. 7 shows the signal on the seed pixel (central) and on the extreme pixel plotted versus estimated impact position for a 17-μm pitch three-pixel cluster.

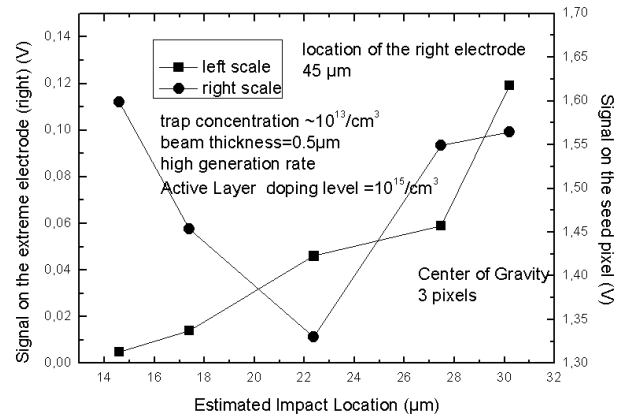


Fig. 7: Signal on the seed and extreme pixel versus estimated impact location. A Center Of Gravity (COG) method on three-pixel clusters is used for the impact determination. For trap concentrations corresponding to fluences of $10^{12}/10^{13} \text{ n/cm}^2$, the signal vanishes dramatically on the extreme electrode limiting its role in the impact reconstruction.

B. Neutron induced defects and downscaling

The Total charge on the three pixel-clusters is simulated for a vertical impact on the cluster at mid-point between the right and central pixel. These 2D simulations have been made for decreasing pixel pitch 30 μm , 15 μm , and 7.5 μm .

Fig. 11: Total charge on three pixels plotted versus neutron fluence for decreasing pitches. The structures are narrow (scaled to the pitch).

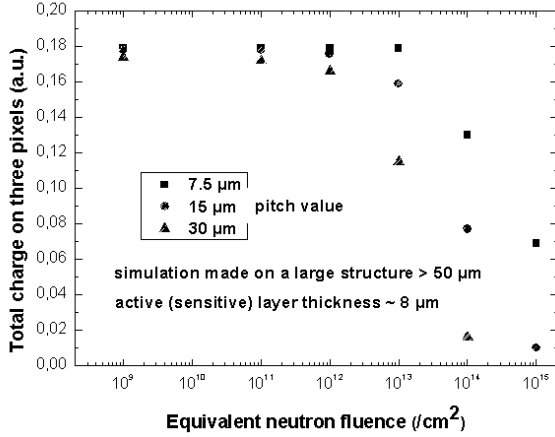


Fig. 12: Total charge on three pixels plotted versus neutron fluence for decreasing pitch values. The structures are large (>50 μm for the 7.5 μm pitch) and more than 150 μm for the 30 μm pitch.

Fig. 11 shows clearly that the increase in the pixel pitch and the lateral dimension of the structure induces a decrease of the radiation tolerance of the structure. Low pixel pitch result in a significant increase of the total signal. In Fig. 12, made with a constant high lateral dimension, the total signal at low fluences does not depend on the pitch but the same conclusion as in Fig. 11 holds for the radiation effects. Downscaling pixel pitch benefits to tolerance to displacement damage. This is due to the reduced ratio between carrier migration length (which reduces when the trap concentration grows) and the dimensions of each pixel.

Similar comments can be made on the systematic reconstruction error plotted versus neutron fluence (Fig.13).

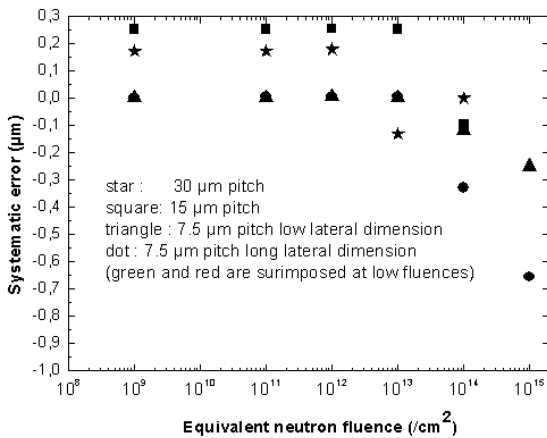


Fig. 13: Systematic error due to reconstruction plotted versus neutron fluence for decreasing pitch values. The effect of the simulation structure lateral dimension is displayed for the lowest pitch. For the other pitches the lateral dimension is taken as large as possible.

It is clear that the systematic error is reduced by downscaling too. The effect of displacement damage seems to have a limited influence on systematic error degradation.

V. EFFECT OF ELECTRODE DIMENSIONS

2D simulations can be used to study the influence of the dimensions of the collecting electrodes of the signal build-up. For a 0.5 μm deep electrode, the signal and the charge is plotted against one lateral dimension (Fig 14.), the extra (2D>3D) dimension being set to 1 μm implicitly by the simulation code.

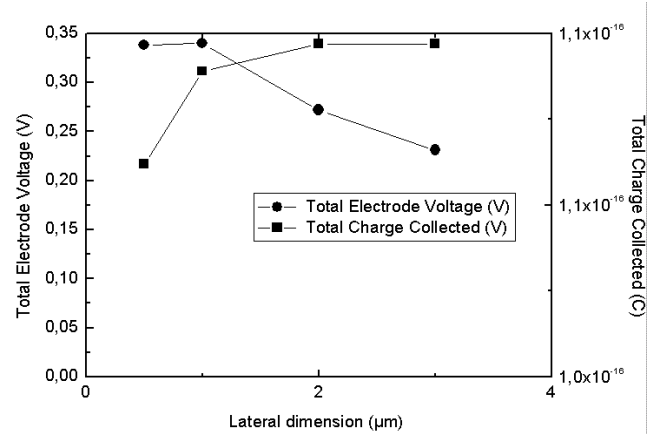


Fig. 14: Signal on three pixels plotted versus electrode lateral dimension. The pitch is 7.5 μm . The neutron fluence is $\sim 10^{12}$ cm^{-2} . Large structures are used for the simulation. 1 μm is the implicit size in the third dimension.

The total charge collected on the three electrodes depends very weakly on the lateral dimension if this is higher than 1 μm . Conversely, the total signal decreases slightly with the lateral dimension, this being due to the increase in the capacitance of the electrode. An optimum appears for a lateral dimension of around 2 μm for which any further size increase does not result in a collected charge increase for the three pixels. It should be reminded that the true total signal depends on the overall capacitance at the electrode node this including the readout input capacitance which is much higher than the sole electrode capacitance.

One can evaluate the influence of the depth of electrode implant (n-well) on the total signal build-up (Fig. 15).

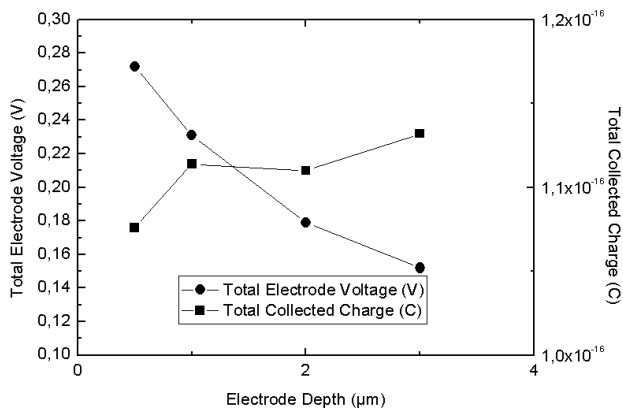


Fig. 15: Signal on the three pixels versus well depth for a $2 \times 1 \mu\text{m} \times \mu\text{m}$ rectangular n-well. The neutron fluence is $\sim 10^{12} \text{ cm}^{-2}$. The pitch remains $7.5 \mu\text{m}$ and a large structure is used.

As well as for the lateral dimensions, the charge collected on the three electrodes is weakly dependent on the electrode depth, the apparent effect on the signal being exclusively due to the increase in the electrode capacitance.

This dimension study provides the necessary information for the optimization of the size of the sensing diode. It is clear that for the present structure the optimum lays around $7.5 \mu\text{m} \times 7.5 \mu\text{m}$ pixels with $2 \mu\text{m} \times 2 \mu\text{m}$ single sensing diodes.

VI. CONCLUSIONS

Present 2D simulation results demonstrate that simulation is an excellent tool to study radiation damage in MAPS (as in [24]) and a necessary step in MAPS development. Simulation results are consistent with established experimental data. Optimization of doping levels in the active layer of the Pixel is achievable using TCAD. At realistic native deep trap concentrations simulation show that $20\text{-}30 \mu\text{m}$ is the upper limit for satisfactory operation of MAPS for charged particle detection. Moreover reduced lateral and vertical dimension result in a confinement effect that makes insulated pixels (i.e. SOI pixel for instance) an alternative option. Three pixel-clusters in 2D are sufficient make an efficient impact point reconstruction even at small pitches. Increasing the active layer thickness is not necessary: it may be scaled down with the lateral dimensions and pitch. Reducing the pitch both benefit to the readout speed and to the displacement damage hardness. Up to now, there is no apparent limit to the downscaling of the pixels' dimensions. MAPS operation should be either improved or unchanged.

Hope remains for the operation of MAPS based detectors at higher hadron fluences if downscaling proves satisfactory. In addition, for low pitches purely binary readout would then be sufficient to obtain micron range resolution. "One pixel hit" operation would be possible simplifying readout, pixel circuitry and data processing.

Downscaling the pixel dimensions is therefore part of a roadmap for future MAPS developments as part as a μVertex detector for future high energy physics experiments.

ACKNOWLEDGMENTS

The author is grateful to A. Ferron (Silvaco) for his advice. The author wishes to thank P. Micout and his coworkers for continuous assistance in software questions and is indebted to the teams of CCALI/IN2P3/IRFU for their assistance.

REFERENCES

- [1] R. Turchetta, J.D Berst, B. Casadei, G. Claus, C. Colledani, W. Dulinski, Y. Hu, D. Husson, J.P. Le Normand, J.L. Riester, G. Deptuch, U. Goerlach, S. Higuere, M. Winter, Nucl. Inst. and Meth. In Phys. Res. A, Volume 458, Issue 3, 11 February 2001, Pages 677-689
- [2] D. Husson, Nucl. Inst. and Meth. In Phys. Res. A 461 (2001) 511-513
- [3] N.T. Fourches, M. Besançon, Y. Li, P. Lutz and F. Orsini, Nucl. Inst. and Meth. In Phys. Res. A 576 (2007) 173-177
- [4] J.M. Heuser, <http://www.gsi.de/documents/DOC-2008-Sep-6-1.pdf>
- [5] M. Ahmed, S.J. Watts, J. Matheson, A. Holmes-Siedle, Nucl. Inst. and Meth. In Phys. Res., A 457 (2001) 588-594
- [6] V. Eremin, A. Ivanov, E. Verbitskaya, Z. Li, S.U. Pandey, Nucl. Inst. and Meth. In Phys. Res. A 426 (1999) 120-125
- [7] V. Eremin, E. Verbitskaya, Z. Li, Nucl. Inst. and Meth. In Phys. Res. A 476 (2002) 537-549
- [8] R.M. Fleming, C.H. Seager, D.V. Lang, E. Bielejec and J.M. Campbell, Appl. Phys. Lett. 90, 172105 (2007)
- [9] R.M. Fleming, C.H. Seager, D.V. Lang, P.J. Cooper, E. Bielejec and J.M. Campbell, J. Appl. Phys. 102, 043711 (2007)
- [10] E. Fretwurst, V. Eremin, H. Feick, J. Gerhardt, Z. Li, G. Lindström, Nucl. Inst. and Meth. In Phys. Res. A 388 (1997) 356-360
- [11] E. Fretwurst, C. Dehn, H. Feick, P. Heydarpoor, G. Lindström, M. Moll, C. Schütze, T. Schulz, Nucl. Inst. and Meth. In Phys. Res. A 377 (1996) 258-264
- [12] I. Kovacevic et al., J. Phys.: Condensed. Matter 17 (2005) S2229-S2235
- [13] G. Kramberger, V. Cindro, J. Mandic, M. Mikuz, M. Zavrtanik, Nucl. Inst. and Meth. In Phys. Res., A 516 (2004) 109-115
- [14] Z. Li, C.J. Li, V. Eremin, E. Verbitskaya, Nucl. Inst. and Meth. In Phys. Res. A 388 (1997) 297-307
- [15] Z. Li, C.J. Li, V. Eremin, E. Verbitskaya, Nucl. Inst. and Meth. In Phys. Res. A 377 (1996) 265-275
- [16] M. Moll, E. Fretwurst, M. Kuhnke, G. Lindström, Nuclear Inst. and Meth. In Phys. Res. B 186 (2002) 100-110
- [17] D. Passeri, P. Ciampolini, G.M. Bilei, Nuclear Inst. and Meth. in Phys. Res. A 439 (2000) 270-274
- [18] QI-Yuan Wang, Jian-Hua Wang, Hui-Fang Deng, Lan-Ying Lin, Microelectronic Engineering 66 (2003) 333-339
- [19] C.H. Seager, R.M. Fleming, D.V. Lang, P.J. Cooper, E. Bielejec, J. M. Campbell, Physica B, Vols 401-402, (2007) Pages 491-494
- [20] H.J. Stein and R. Gereth., J. Appl. Phys. 39, 6, 2890 (1968)
- [21] N. Fourches, J. Appl. Phys. 77(8) 3684 (1995)
- [22] N. Fourches, Y. Degerli, M. Besançon, A. Besson, G. Claus, G. Deptuch, W. Dulinski, M. Goffe, A. Himmi, C. Hu-Guo, P. Lutz, M. Rouger, I. Valin, M. Winter. IEEE NSS Conf. Rec. N4-7, 93 (2005)
- [23] Y. Degerli, A. Besson, G. Claus, M. Combet, A. Dorokhov, W. Dulinski, M. Goffe, A. Himmi, Y. Li, F. Orsini, IEEE NSS Conf. Record, N24-254 (2007)
- [24] E.G. Villani, P.P. Allport, G. Casse, A. Evans, M. Tyndel, R. Turchetta, J.J. Velthuis, IEEE NSS Conf. Record, 1222-1226, Vol 2 (2004)